

Combined production of electricity and hydrogen from solar energy and its use in the wine sector

Javier Carroquino^{1,3}, Vicente Roda^{2,4}, Radu Mustata², Jesús Yago³, Luis Valiño²,
Antonio Lozano², Félix Barreras^{2,†}

¹ *University of Zaragoza, Dep. of Electrical Engineering, Maria de Luna 3, 50018 – Zaragoza (Spain)*

² *LIFTEC, CSIC-Univ. of Zaragoza, Maria de Luna 10, 50018 – Zaragoza (Spain)*

³ *Intergia Energía Sostenible S.L., Av. Cataluña 19, 50014 – Zaragoza (Spain)*

⁴ *Present address: Institut de Robòtica i Informàtica Industrial, CSIC-UPC, Llorens i Artigas 4-6, 08028 – Barcelona (Spain)*

ABSTRACT

In the present research, the energy demanded by the wastewater treatment plant of a winery and the pumping station of the irrigation system of a vineyard is supplied by a stand-alone renewable energy system formed by three photovoltaic arrays connected to a microgrid. A relatively small battery maintains the stability and quality of the energy supply acting as a short-term energy storage. Hydrogen is generated in a production and refueling plant specifically designed for this project, and it is eventually used in a plug-in BEV properly modified as a hybrid vehicle by adding a PEM fuel cell. On the one hand, the technical and economic feasibility of the on-site electricity production for the winery and vineyard, compared to the commercial electricity from the grid and diesel gensets, is demonstrated. On the other hand, the diesel savings by the hydrogen generated on site are assessed. The electricity (72 MWh) and hydrogen (1,214 m³) produced in the first year have saved the emission of around 27 tons of equivalent CO₂.

Keywords: Power-to-gas; Renewable energy; Solar PV energy; Hydrogen; PEM fuel cell;
Hybrid electric vehicle

[†] Corresponding Author: felix@litec.csic.es
Ph.: (+34) 976 506 520. Fax: (+34) 976 506 644

NOMENCLATURE

Acronyms

ATEX	Anti-explosion elements
BEV	Battery electric vehicles
CO ₂ -e	equivalent CO ₂
ECU	Electronic control unit
EM	Electric machine of the BEV
EMS	Energy Management System
FC	Fuel cell
FCHEV	Fuel cell hybrid electric vehicles
GSS	Gas storage system
HEV	Hybrid electric vehicle
HPP	Hybrid power plant
HRES	Hybrid renewable energy systems
IRR	Internal rate of return (%)
NI	National Instruments
NPV	Net present value (€)
OS	Operative system
PEM	Polymer electrolyte membrane
PLC	Programmable logic controller
PV	Solar photovoltaic
PWM	Pulse-width modulation
RES	Renewable energy sources
SOC	State of charge of the battery
TAC	Total annual costs
WWTP+IS	Waste water treatment plant and irrigation system

Latin symbols

<i>AE</i>	Annual expenses (€)
<i>C</i>	Cash-flow
<i>CoE</i>	Energy cost (€)
<i>CoL</i>	Cost due to lifetime (€)
<i>CoP</i>	Power cost (€)
<i>E</i>	Energy consumed (kWh)
<i>I_o</i>	Initial investment costs (€)
<i>Inf</i>	Inflation (%)
<i>k</i>	Discount rate
<i>P</i>	Power consumed (kW)

Subscript

<i>Bat</i>	Battery system
<i>CE</i>	Commercial energy
<i>DG</i>	Diesel generation set
<i>Gen</i>	General
<i>Inv</i>	Inverters
<i>PV</i>	PV solar plant

1. Introduction

Increasing the use of renewable energy sources (RES) in the energy mix has become a challenge for power engineers and scientists all over the world. Even when hybrid power systems based on RES (HRES) have attracted the attention of the sustainable energy market, the optimal use of either solar photovoltaic (PV) or wind power is difficult, specifically in local power grids. This is because of their fluctuating and intermittent nature, due to the dependence on meteorological conditions. Thus, standalone renewable energy sources cannot guarantee a reliable power supply. A typical solution to this problem is the use of HRES combining both short-term energy storage options (batteries, capacitors, flywheels, or compressed air) and long-term ones with hydrogen as energy storage. Hydrogen is considered the energy vector of the future, especially if it is produced from RES [1-5]. Different energy storage systems have been used to optimize the energy management of power systems based on single or multiple RES in the household sector, in applications such as plug-in battery electric vehicles (BEV) [6] or fuel cells [7-10].

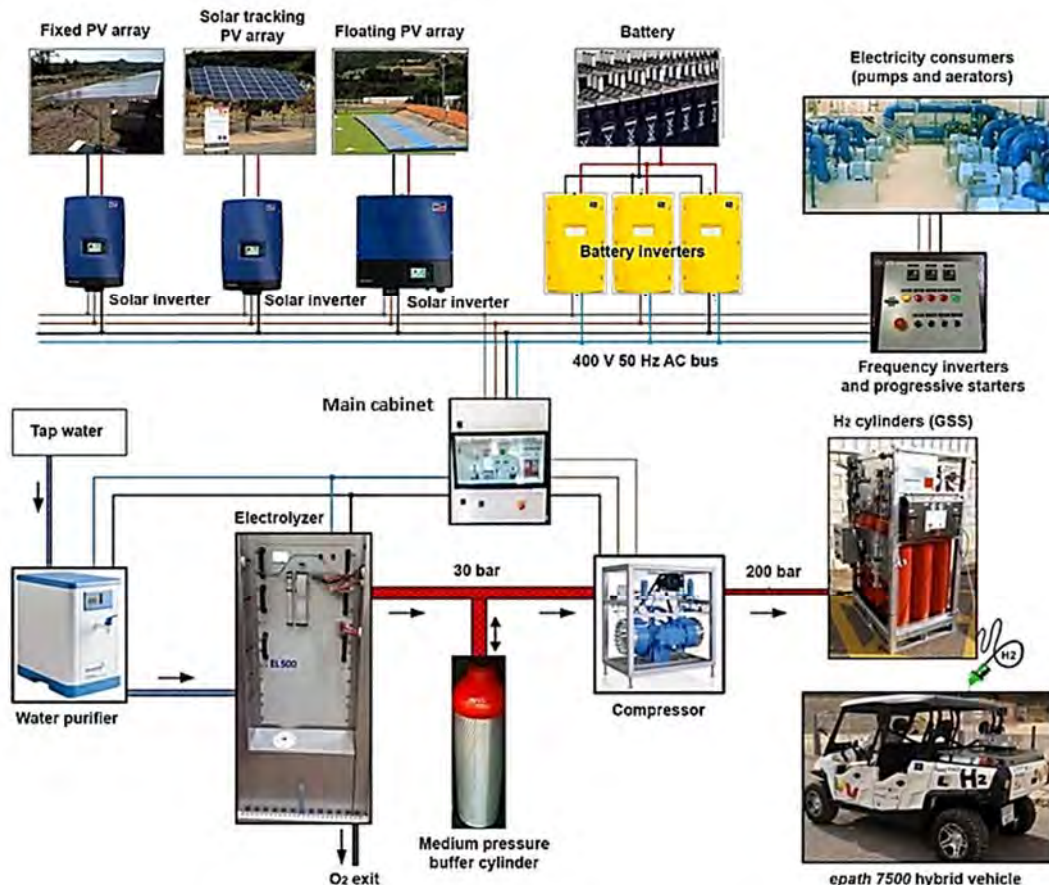
In remote rural areas, the energy demand can be actually satisfied using HRES, but their introduction has been limited by the lack of economic viability and technical adaptation. Aerial power lines, which are very expensive, are normally extended in natural areas to distribute commercial electricity to the consumers. These infrastructures have a severe environmental impact affecting the skyline and, what is more important, killing both native and migratory birds, something especially serious in the case of endangered species. In the particular case of the wine industry, energy demands (irrigation, farming machinery, thermal processes, mobility, etc.) present strong seasonal cycles not only throughout the year but also during the day. Besides, fossil fuels are massively used both in transportation and on-site power generation, emitting CO₂ and other pollutants. Thus, in order to achieve standalone HRES with high reliability, which would contribute to their massive use in the wine sector, both short-term and long-term energy management systems must be considered [11,12].

In this research, a part of the energy demanded in a winery is supplied by the power produced from a PV energy system. Specifically, it includes the power consumed by the wastewater treatment plant (aerators), the pumping system for sludge, filtering and irrigation processes, a hydrogen production and refueling station, and the recharge of

33 the battery system of an electric vehicle. To the authors' knowledge, this is the first time
 34 that such challenge is assumed in this specific sector, which is very relevant for the
 35 European countries of the Mediterranean area (Italy, France, Greece, Spain, Portugal,
 36 etc.). The research describes in depth the design and operational tests performed during
 37 the demonstration period of the PV system and the hydrogen production and refueling
 38 station. Besides, the performance of a BEV suitable modified into a hybrid electric
 39 vehicle (FCHEV) equipped with a polymer electrolyte membrane fuel cell (PEMFC) is also
 40 discussed.

41 2. Description of the different facilities

42 This research is part of the project *"Profitable Small Scale Renewable Energy*
 43 *Systems in Agrifood Industry and Rural Areas: Demonstration in the Wine Sector"* [13],
 44 funded by the European Union under the LIFE program.



45

46

Figure 1. General scheme of the power-to-gas plant of this project

47

48

The project facility is placed at Viñas del Vero winery, which is located in the Somontano region, in the north of Aragon (Spain). As depicted in Fig. 1, this power-to-

49 gas power plant is formed by two main facilities: the electricity production section
 50 (upper row) and the hydrogen production and storage units (lower row). They are
 51 interconnected by a main cabinet where all the control and safety software are installed.
 52 The surplus electricity produced by a solar PV plant is converted into hydrogen by water
 53 electrolysis. The hydrogen produced is stored in pressure cylinders and is further
 54 reconverted into electricity in a PEMFC that is the secondary power source of the hybrid
 55 power plant of a FCHEV.

56 **2.1. The electrical facility**

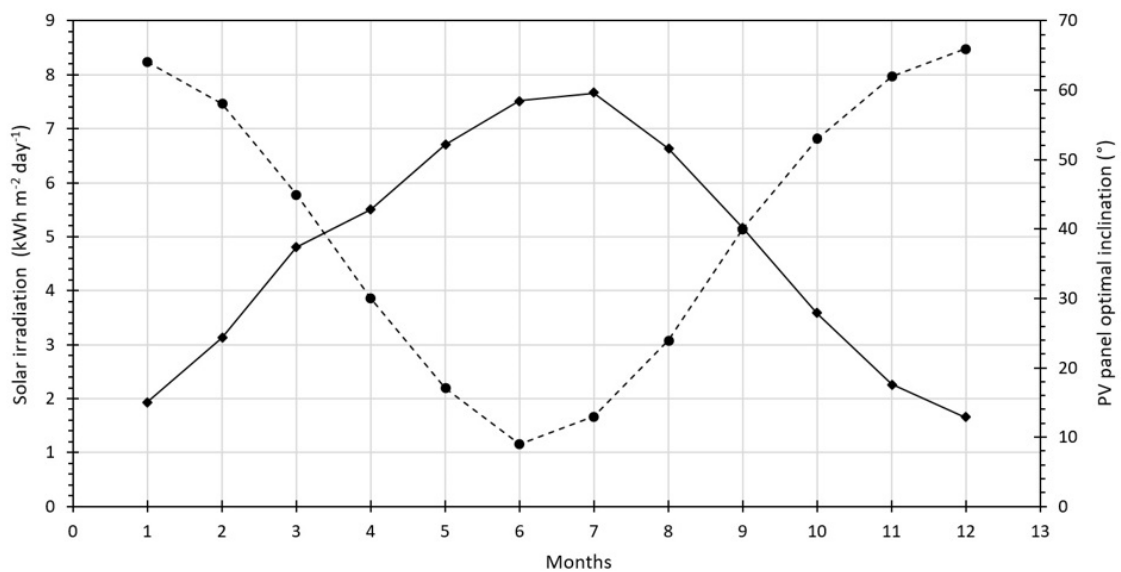
57 The energy consumed by the wastewater treatment plant and the irrigation system
 58 (WWTP+IS), which was originally connected to the main winery electric grid, has been
 59 replaced by a solar PV plant and a microgrid formed by battery storage system. As
 60 depicted in Fig. 1, the stand-alone electrical facility is formed by the PV plant, a battery
 61 that acts as the short-term energy storage system, different inverters to properly use
 62 the electricity, and the consumer elements. The water used for irrigation is recycled
 63 from the wine production processes. The wastewater is accumulated in an aeration
 64 pond where it is treated, and is sequentially moved using centrifugal pumps to the
 65 filtration sandbox and to the irrigation pond. The vineyards to be irrigated have an area
 66 of 10 ha, and the annual water volume used for this purpose reaches 10,000 m³ [14].
 67 The power consumed and tasks performed by the different consumers are summarized
 68 in Table 1.

Consumers	Qty	Tasks	Total Power (kW)
Aerators	2	Injecting air bubbles to activate the biodegradation of the waste water	28
Elevation pumps	2	Moving the treated water from the different ponds	9.8
Irrigation pump	1	Irrigating the vineyard during the irrigation season (123 days)	11
Sludge pumps	2	Moving the sludge from aeration pond to the sludge one	3.6

69 Table 1. Summary of the electrical loads of the WWTP+IS

70 Among the different possible RES, only solar and wind power were initially
 71 considered, since there are no other reliable resources in the area. However, wind

72 power was discarded due to the small average air velocity (1.66 m s^{-1}) measured during
 73 on-site measurement campaigns [15]. On the contrary, solar power is a very reliable
 74 option due to the high average solar irradiance in Spain [16]. The average value
 75 corresponding to the exact location of the winery, obtained from the Photovoltaic
 76 Geographical Information System (PVGIS) of the European Union [17], is 4.73 kWh m^{-2}
 77 day^{-1} , as can be observed in Fig. 2. The maximum value takes place in Summer,
 78 concurring with the irrigation season, and it is well above $7.5 \text{ kWh m}^{-2} \text{ day}^{-1}$. In addition,
 79 optimal inclination according to PVGIS varies between 9° in June and 66° in December,
 80 with an annual average value of 37° .



81
 82 Figure 2. Estimated values of solar irradiation (solid line) and optimal panel inclination
 83 (dashed line) for each month at the winery area [25]

84 2.1.1. The solar photovoltaic system

85 The use of solar energy within the energy mix is common in many countries all over
 86 the world [18-23]. However, the indisputable role of solar energy in the Twenty-first
 87 Century is overshadowed by the intermittent nature of its power production. This
 88 problem can be addressed by the use of both short-term and long-term energy storage
 89 systems [24-29]. Although conventional stand-alone solar systems often use a DC bus
 90 architecture, it was decided to design a system with an AC bus, to which both PV
 91 inverters and power consumers are connected. So, the electric power produced by the
 92 PV panels can be directly used by the different AC consumers using DC/AC solar power
 93 inverters, increasing the efficiency of the electric system, and reducing the battery size.



94

95

Figure 3. Assembling of the different solar arrays and main project booth at the

96

WWTP+IS area

97

There are several computational tools to assist the design and analysis of HRES and microgrids, such as the Hybrid Optimization Model for Electric Renewables (HOMER), improved Hybrid Optimization by Genetic Algorithm (iHOGA), and Hybrid2, which implement quantitative methods. In the present research, to optimize the design and performance of the system in terms of efficiency and reliability, iHOGA was used. In essence, this software tool incorporates the Ah ageing model to optimize the HRES, and takes advantage of genetic algorithm characteristics to enhance the whole optimization process, giving good results in a short computational time [30]. The power plant includes three sets of PV panels, in order to show different assembling options and to carry out comparative studies: a fixed structure located on the sandbox, a solar tracker, and a floating set placed on the surface of the aeration pond. The location of all PV arrays in the WWTP+IS area is indicated in Fig. 3. All of them are commercial (multicrystalline) polysilicon TP 265/275 Wp model PV panels manufactured by REC, which have a conversion efficiency of 16.1% and 16.7%, respectively. A summary of the main data of the three technologies is presented in Table 2. Regarding to the fixed structure, the tilt of the PV panels can be set to 5° or 30° in order to adapt the profile of the incident solar irradiation to the different energy seasonal profiles. With respect to the floating PV array, it should be noted that a remarkable advantage of the decision to place it over the surface of the aeration pond is that the performance of the panels is increased when

115

116 its working temperature is decreased. In addition, both evaporation of water and
 117 proliferation of algae in the pond are also reduced. In summary, the total solar power
 118 installed reaches 43.2 kWp.

Array	Supporting structure	Tilt	PV power (kWp)
Fixed	Metallic structure on the ground	5° or 30°	10.8
Tracking	Two-axis solar tracker	-	10.8
Floating	Structure designed for this application	5°	21.6

119 Table 2. Main characteristics of the different arrays forming the solar PV plant

120 The variable voltage and intensity DC produced by the PV panels is converted to
 121 three-phase AC (400 V, 50 Hz) using three DC/AC Sunny Tripower (STP) PV solar inverters
 122 from SMA. Their electrical connection to the main AC bus is depicted in Fig. 1.

123 **2.1.2. The battery storage system**

124 The total energy produced by the solar PV facility normally exceeds the needs of the
 125 WWTP+IS. A short-term storage system allows energy to be available at any time of the
 126 day and at night, regardless of the generator instantaneous production. It consists in a
 127 lead-acid battery bank with 24 solar.power OPzS 3610 cells manufactured by Hoppecke,
 128 with a capacity of 2,680 Ah (128.64 kWh). They are formed by tubular plates with liquid
 129 electrolyte, suitable for this application since ultra-fast discharge regimes are not
 130 expected. Three Sunny Island SI-8.0H battery inverters from SMA (one for each phase)
 131 are used to produce a 400 V 50 Hz microgrid and to correctly manage the battery charge
 132 and discharge processes. Their electrical connection to the main AC bus can be observed
 133 in Fig. 1. The battery storage system provides flexibility to the facility by storing the
 134 excess energy to be consumed later during the periods of lack and/or low renewable
 135 energy production.

136 There are several factors that affect the initial investment and maintenance costs
 137 of the battery. The variability of the solar PV system and the operating philosophy can
 138 impose stress conditions that eventually reduce its lifetime. On the one hand, the
 139 smaller the size of the battery bank the higher the cost effectiveness of the whole
 140 system. On the other hand, the lifetime of lead-acid batteries depends on the depth of
 141 discharge and the number of cycles. Lowering a state of charge (SOC) below 20% can be
 142 very harmful. For this reason, a key point when designing this HRES was to reduce the

143 amount of energy to be stored in the battery bank. It is for this reason that in this system
144 the capacity of the battery bank was not calculated to provide a large autonomy, but to
145 match the production and consumption in an intraday regime, with a small depth of
146 discharge. On the contrary, on days with low PV production, a deeper discharge cycle is
147 possible, but this situation is very uncommon. The actual SOC of the battery is calculated
148 by the charge controller with an accuracy of 95% by combining the direct measurement
149 of the in-flowing and out-flowing current with a current voltage model.

150 **2.1.3. Energy management system and control strategy**

151 The implementation of an energy management system (EMS) is required both to
152 avoid failures due to the lack of available energy and to minimize losses when it cannot
153 be used nor stored [29]. It is noteworthy that much of the consumption of the system
154 can be deferred. Consequently, the loads can be activated when there is PV energy
155 production and deactivated when the battery has a low state of charge. To maximize
156 the output power from the PV modules to the direct consumers, the maximum power
157 point (MPP) control unit is employed [31]. To this end, a fuzzy logic control is used for
158 the solution of the different options of the nonlinear system. The system is managed in
159 such a way that the energy is consumed, if possible, when it is generated, avoiding its
160 cycling in the battery. As a result, the energy stored is largely reduced, minimizing the
161 inherent losses for AC to DC to AC conversion in the battery inverters and those for the
162 battery charge and discharge processes.

163 The EMS designed in this project optimizes the match between the load demand
164 and the energy generated by the RES at every time. For this purpose, several decisions
165 were adopted in order to establish the priorities between the use of the different
166 consumers and the production of hydrogen during each day, taking into account the
167 different seasons of the year. Different sensors measure the solar irradiation, the energy
168 production, and the SOC of the battery, among other variables. With all of them, the
169 EMS activates or deactivates the different loads. Finally, as far as energy efficiency is
170 concerned, the electric motors of the different loads are driven by commercial variable
171 frequency drivers. Thus, the aerators and the pumps not only work at the optimum
172 working point of their load curve, but also current peaks are avoided, smoothing their
173 mechanical and electrical operation and enlarging its useful lifetime.



174

175

Figure 4. Inside (left) and outside (right) images of the main control cabinet

176

177

178

179

180

181

182

183

184

185

186

187

The control and safety software is loaded in a computer inside the main cabinet that interconnects the electrical and hydrogen facilities. Two pictures of the inner and outer sides of this cabinet are depicted in Fig. 4. All the decisions adopted are included in the NI LabView® control software that runs on an industrial computer with Windows 7 OS. It is an ultracompact Epatec IPC computer (number 1 in Fig. 4) with a fast Intel Celeron 1.8 GHz Quad Core processor. The Arduino PLC automata (number 2 in Fig. 4) is a M-duino 57 R with an ATmega2560 microcontroller and a clock speed of 16 MHz. It has 18 input ports (12 for analog/digital signals, and 6 interrupt switches), as well as 39 output points (8 analog signals, 23 digital ones, and 8 PWM isolated 8 bit). Users can interact with the control and supervision system through a commercial touch screen. The visualization software shows the status of the installation using different windows that can be easily displayed. Remote access via internet is also possible.

188

2.2. The hydrogen facility

189

190

191

192

193

194

In addition to the short-term energy storage battery, in the present project hydrogen is used as a long-term storage system. It should be noted that here, contrary to the most common solution where the stored energy is reverted to the same system, hydrogen energy is used to refuel a plug-in BEV properly modified to a hybrid one using a PEM fuel cell. The hydrogen facility is formed by a production and refueling plant and the FCHEV that is the end-user of the produced hydrogen.

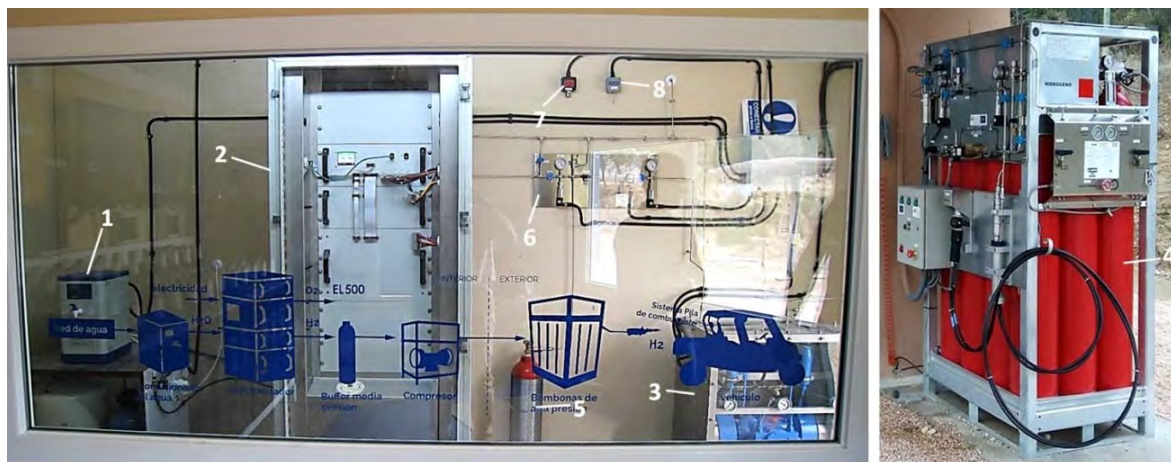
195 **2.2.1. The hydrogen production and refueling plant**

196 The hydrogen generation and refueling station (see Fig. 5) has been specifically
 197 designed for this research. The system is mainly composed by a compact water
 198 purification system (1), an alkaline electrolyzer (2), a metal diaphragm compressor (3),
 199 and a stationary gas storage system (4), and a medium-pressure buffer aluminum
 200 cylinder from Luxfer with a water volume of 10 liters (5) which is placed just in between
 201 the electrolyzer and the compressor. The main characteristics of these equipment are
 202 summarized in Table 3.

Equipment	Manufacturer	Technology	Characteristics
Ecomatic water purification system	Wasserlab	Reverse osmosis	Flow: 3 l h ⁻¹ ; Conductivity: < 5 μS cm ⁻¹
Electrolyzer EL-500	Heliocentris	Alkaline Exchange Membrane (KOH)	Flow: 500 NI h ⁻¹ @ 30 bar; Purity: 99.999%
Compressor MV6208	Sera	Metal-diaphragm, double-stage	Flow: 500 NI h ⁻¹ @ 200 bar

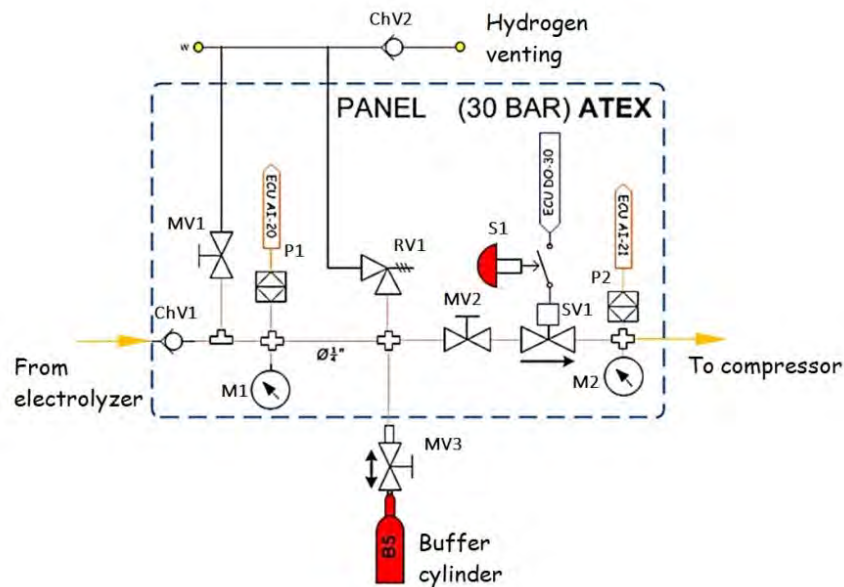
203 Table 3. Equipment of the hydrogen production plant

204 All equipment, devices and elements for the hydrogen production plant are
 205 installed in an isolated room inside the project booth, while those corresponding to the
 206 storage and refueling station are placed outside. To avoid possible accidents, all
 207 elements and devices fulfill the anti-explosion (ATEX) regulations required for any
 208 hydrogen facility. A detector for hydrogen leaks (7), and a temperature sensor (8) are
 209 also assembled to ensure the safe operation of the facility.



210
 211 Figure 5. Hydrogen production and refueling plant. Pictures of the production devices
 212 assembled inside the booth and the stationary GSS placed outside (right)

213 The flow diagram of the control panel (number 6 in Fig. 5) can be observed in Fig. 6.
 214 It is formed by two check-valves (ChV1, ChV2) for the correct circulation of hydrogen,
 215 two manometers (M1, M2) to visualize the pressure just after the electrolyzer and
 216 before the compressor, respectively, and three manual valves (MV1, MV2, MV3) that
 217 are assembled for security.



218
 219 Figure 6. Panel used to control the correct performance of the compression stage

220 The safe operation of the compressor is controlled by the electrical signal provided
 221 by the solenoid valve SV1 that takes the pressure reference from pressure transducers
 222 P1 and P2. It is turned on when the pressure at P2 raises to 29.5 bar and turns off when
 223 it falls below 15 bar. The panel also includes an automatic hydrogen release valve (RV1)
 224 that is activated when the pressure at the inlet point (P1) is above 45 bar.

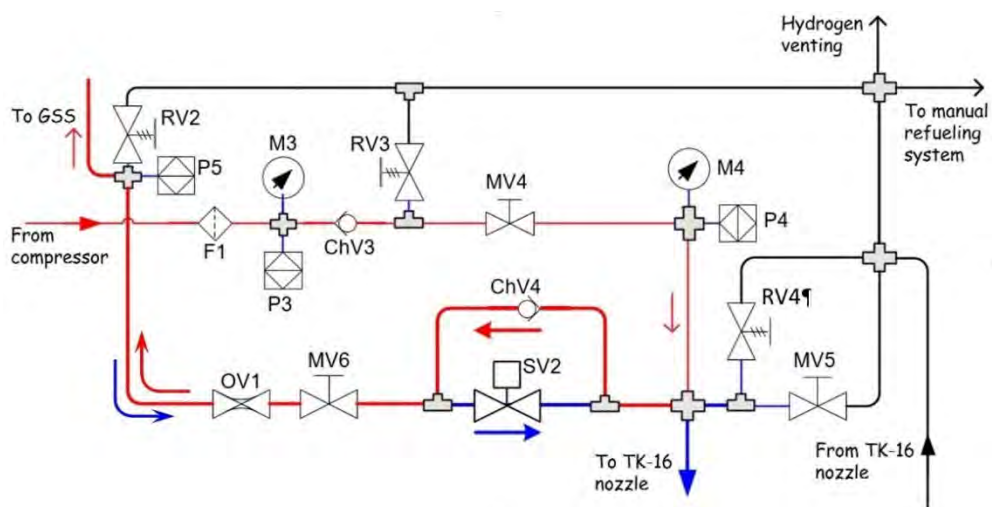
225 The hydrogen plant also includes a stationary gas storage system (GSS) formed by a
 226 rack with 12 cylinders, with a water volume of 50 l each. Thus, it can store 106 m³ (9.53
 227 kg) of hydrogen at 200 bar. The H₂ stored at the stationary GSS is automatically supplied
 228 to the FCHEV with a commercial WEH[®] refueling system. It is formed by a TK-16 nozzle
 229 and a TN-1 receptacle, and integrates a high-flow check valve and a 20 μm self-cleaning
 230 particle filter. The WEH system has also a breakaway coupling that cuts off the hydrogen
 231 flow if a force greater than 300 N is exerted on the hose, preventing it for breaking. A
 232 connection panel with its corresponding control electronics was specifically designed
 233 and built for this application. It is placed on one side of the GSS, and a photo and the
 234 corresponding flow diagram is depicted in Fig. 7. It is formed by a coalescent filter (F1),

235 and different check (ChV3, ChV4) and release valves (RV2, RV3, RV4). As a novelty, it has
 236 been designed both to refill the stationary GSS with hydrogen from the compressor (red
 237 lines) and to discharge it to refuel the GSS of the FCHEV (blue lines). Thus, some pipes
 238 of this panel are indistinctly used both for charge and discharge processes. The correct
 239 circulation of the gas is controlled by the solenoid valve SV2. The electrical signal to
 240 activate SV2 when refueling comes from the supplying switch placed at the control
 241 panel. The overflow valve, OV1, cuts off the hydrogen flow if an unexpected high value
 242 is detected providing an extra safety to the facility. This valve also moderates the
 243 flowrate when the solenoid valve SV2 is opened to refuel hydrogen to the GSS of the
 244 FCHEV.



245
 246

a)



247
 248

b)

249 Figure 7. Panel used to refill the stationary GSS and to refuel hydrogen to the FCHEV

250 **2.2.2. The PEMFC hybrid electric vehicle (FCHEV)**

251 The end-user of the hydrogen system is a commercial ePath-7500 electric car
252 manufactured by EMC (see Fig. 8 a), suitably modified to be powered by a hybrid
253 powertrain based on PEM fuel cell and batteries. This is an all-wheel drive 4-seat vehicle
254 designed to travel on bumpy and irregular terrain, ideal for agricultural or industrial
255 tasks. Originally, the 7.5 kW 72 V electric motor of the car was powered by a set of 12
256 gel-type 6 V 225 A-h batteries. The EM is connected to the main DC bus through a DC/AC
257 booster electronic converter. The PEM fuel cell stack with its corresponding GSS, and
258 the electronic devices used for hybridization were assembled at the tilting rear load
259 platform, as shown in Fig. 8 b).

260 A commercial Horizon H-3000 PEMFC stack, with a rated power of 3 kW, was
261 included as the second power source in the HPP. This is an open-cathode stack formed
262 by 72 cells and graphite bipolar plates that includes 4 axial fans that supply the air flow
263 needed for both the electrochemical reactions and to cool the stack down to the
264 working temperature (50-65°C). At the rated power (70 A, 43.2 V), the gross efficiency
265 is 47.4%, which decreases to 41.8% (net) when power consumed by the ancillary systems
266 are considered. The GSS of the FCHEV is formed by four 10 l Luxfer aluminum cylinders,
267 which can store 0.64 kg (7.12 Nm³) of hydrogen when compressed at 200 bar. The
268 supplying system includes a recirculation system formed by a proportional solenoid
269 valve and an ejector that allows to recirculate part of the unreacted hydrogen from the
270 anode sides.



271
272 a)



b)

273 Figure 8. The original ePath 7500 BEV (a), and the remodeled FCHEV (b)

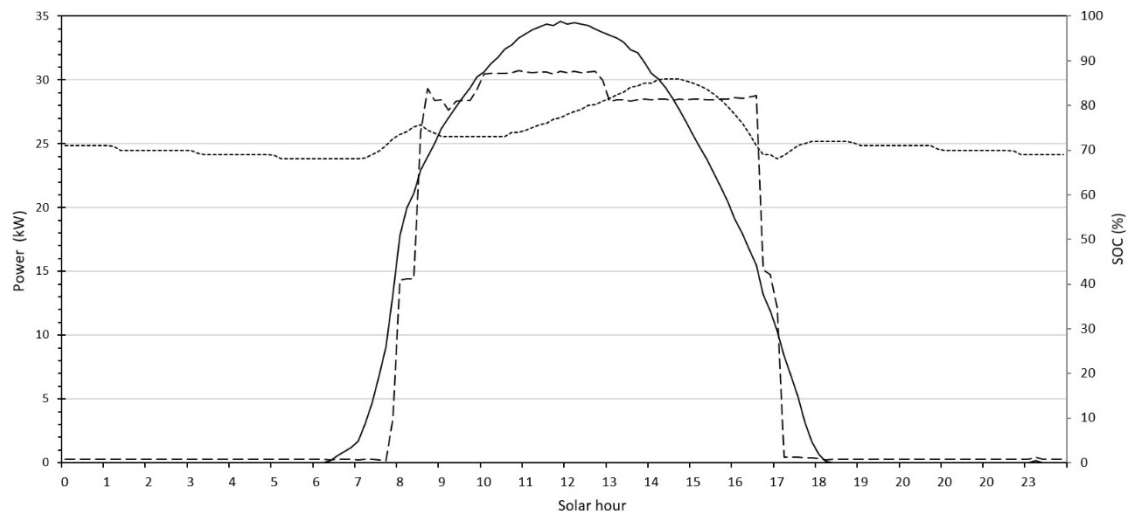
274 The active HPP of the FCHEV is formed by a booster DC/DC power converter that
275 supplies the electric power from the PEMFC stack to the main DC bus, and two other
276 DC/DC converters that deliver power to the different elements of the ancillary systems
277 at 12 V and 24 V. To control and monitor the different electrical parameters of the
278 H₂+PEMFC system, a NI roboRIO microcontroller with a sampling frequency of 800 Hz
279 was used as the central electronic control unit (ECU). The control system includes as a
280 novelty in fuel cells, a discrete state machine model programmed in LabVIEW with LINUX
281 realtime operating system, which was embedded into the ECU microcontroller [32].
282 Basically, there are two main operation states. When the vehicle operates in a low
283 consumption rate and the SoC of the battery is below 95%, the stack is switched to
284 CHARGING mode. In this case, the excess of energy produced by the stack is sent to
285 recharge the battery. On the contrary, if the power demanded at the main DC bus
286 increases, it is shifted to the SUPPLY POWER mode, providing around 30% of the total
287 power demanded by the EM of the FCHEV. To check the correct operation of the stack,
288 a typical polarization curve was also recorded into the ECU. If the PEMFC stack works
289 properly, it alternates between CHARGING and SUPPLY POWER modes. But, if for a given
290 current it is detected that the voltage delivered by the stack differs by 10% from the
291 value of the recorded polarization curve, it is moved to the REHABILITATION mode. In
292 this case a purging sequence is activated in order to remove the water accumulated
293 inside the stack since the commercial H-3000 operates in anode dead-end mode.
294 Usually, after the purging sequence the performance of the stack is recovered and it is
295 again moved to SUPPLY POWER or CHARGING modes, depending on the total power
296 demanded by the vehicle. Otherwise, the stack is eventually shifted to the FINISH mode,
297 stopping the hybrid control sequence.

298 **3. Results**

299 The system described in this paper was fully installed by the end of May 2016, and
300 the main results obtained in this year are discussed below.

301 **3.1. Performance of the electric system**

302 The performance of the PV/electric system for two typical sunny days, one out of
303 the irrigation season, and another within it, are depicted in Figs. 9 and 10, respectively.



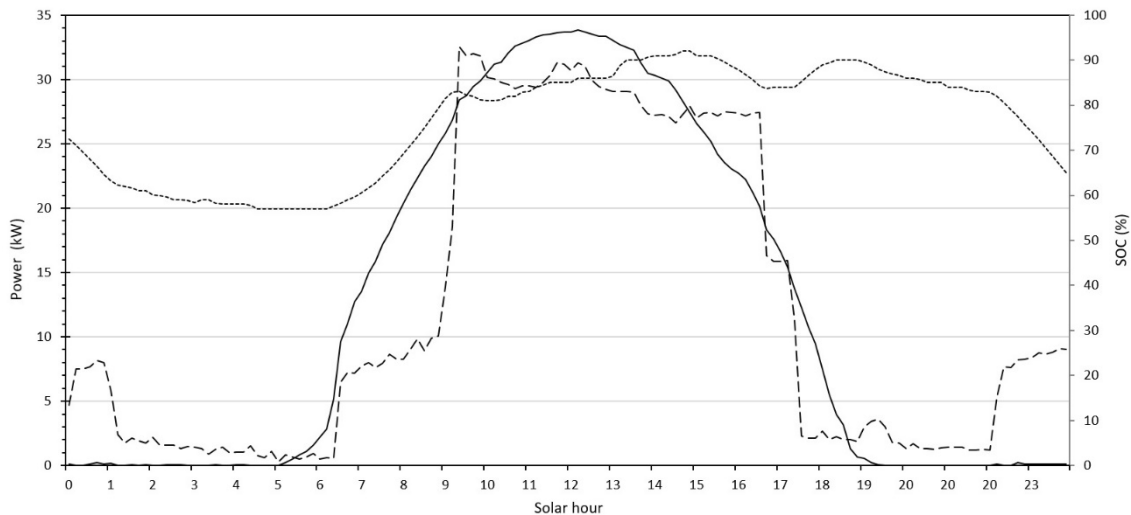
304

305 Figure 9. Electric performance during March 19th 2017, a day out of the irrigation
 306 season. Solid line for power production, dashed for consumption, and dotted one for
 307 the SOC of the battery bank

308 On the one hand, out of the irrigation season, virtually all loads are managed by the
 309 system automatically. Thus, the loads are connected during the day, obtaining the
 310 maximum simultaneity between generation and consumption of energy, as shown in
 311 Fig. 9. It is verified that the energy demand is suitably adapted to the energy production.
 312 Only the area not shared by both the production and consumption curves corresponds
 313 to the energy charged or discharged from the battery. This represents a very small
 314 fraction of the total, minimizing the energy cycled in the battery and the associated
 315 AC/DC and DC/AC conversions, avoiding their corresponding losses. The battery absorbs
 316 the small intra-day differences of production and consumption, with SOC variations less
 317 than 18%, and also maintains its high level of charge which allows the system to work in
 318 cloudy days. The average level of SOC (73%) has not been set too high, since no night
 319 consumption is expected and in anticipation of being able to store energy if the loads
 320 are disconnected part of the day for some reason.

321 On the other hand, during the irrigation season, the irrigation is scheduled by the
 322 vineyard managers, depending on the needs of vine growing. The control system
 323 prioritizes these consumptions and adapts the other ones according to the availability
 324 of energy. The system manages the other loads automatically. In Fig. 10, the main
 325 nocturnal consumption corresponds to the irrigation system. During the first few hours
 326 of sunshine in the morning, a part of the energy produced is used to recharge the

327 battery, compensating for the nighttime consumption. The rest of the day, once the SOC
 328 of the battery is reestablished, the demand is again well-matched to the production of
 329 energy. The SOC variations are less than 35%, and the level of charge is high, which
 330 allows the system to work during the night or in cloudy days. The average level of SOC
 331 (76%) is similar to that obtained outside the irrigation season, but at sunset it is above
 332 90%, waiting for the night consumption.



333
 334 Figure 10. Electric performance during July 28th, 2017, a day within the irrigation
 335 season. The legend is the same as in Fig. 9

336 During the first year the actual electricity produced by the PV system was 71.9
 337 MWh. Part of that energy was used for the different consumers of the WWTP+IS (62.15
 338 MWh), and 6.4 MWh was employed to produce hydrogen. The energy losses in the
 339 system, including those caused by the charge and discharge of the battery bank, have
 340 been only 4.76%. This is a very good performance, due to the optimized management
 341 strategy. To estimate the amount of equivalent CO₂ saved, the energy mix in the Aragon
 342 region has to be considered. Thus, considering an emission factor of 0.385 kg of CO₂-e
 343 per kWh of electricity [33], the emission to the atmosphere of around 27 tons of CO₂ has
 344 been avoided. Besides, during this period, 1,214 Nm³ of hydrogen have been produced.
 345 As the average consumption of hydrogen when moving at 15.6 km h⁻¹ is around 12 NI
 346 min⁻¹ (3.6 Nm³ day⁻¹), considering a diesel specific rate of 15 l per 100 km in a typical
 347 agricultural car, and including the energy supplied by the battery when working in hybrid
 348 mode that needs to be recharged every day, the use of hydrogen in the FCHEV has saved
 349 the consumption of around 1,010 l of diesel. Considering a production factor of 2.539 kg

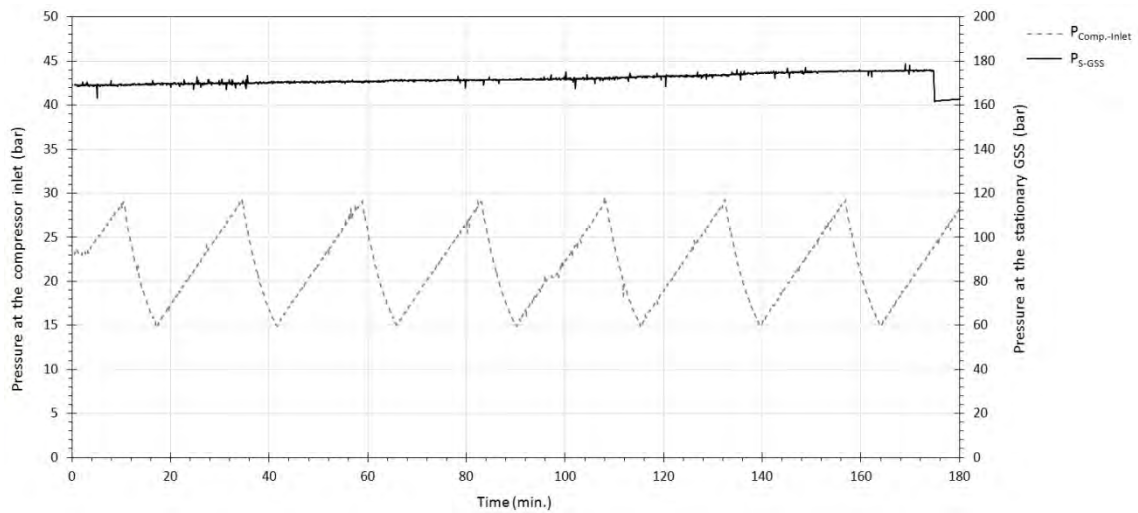
350 of CO₂-e per liter of diesel [34], the emission of 3 tons of CO₂-e has been avoided.

351 Taking into account the efficiency of the different elements of the power-to-gas
352 plant, the overall efficiency for the electricity conversion, from the PV panels to the
353 vehicle wheels, can be estimated. It was obtained that, depending on the electricity used
354 to produce the hydrogen, it ranges from 24.6% to 30.5%. The upper limit is reached
355 when the electricity to produce hydrogen is directly obtained from the PV panels (the
356 conversion efficiency of the DC/AC STP inverters is 98.4%), while the lower one
357 corresponds to hydrogen produced from energy previously stored in the battery. In the
358 last case, the efficiency of the battery inverters (95%) and that of the charge and
359 discharge processes (85%) have to be included in the analysis.

360 **3.2. Performance of the hydrogen production and refueling plant**

361 The behavior of two pressure transducers, P2 (at the compressor inlet) and P5 (at
362 the stationary GSS) of the hydrogen production and refueling plant, is shown in Fig. 11
363 a). The data correspond to a period of 3 hours (from 10:00 to 13:00) that includes the
364 refilling of the stationary GSS with hydrogen produced by the electrolyzer and the
365 refueling of the GSS of the hybrid electric vehicle.

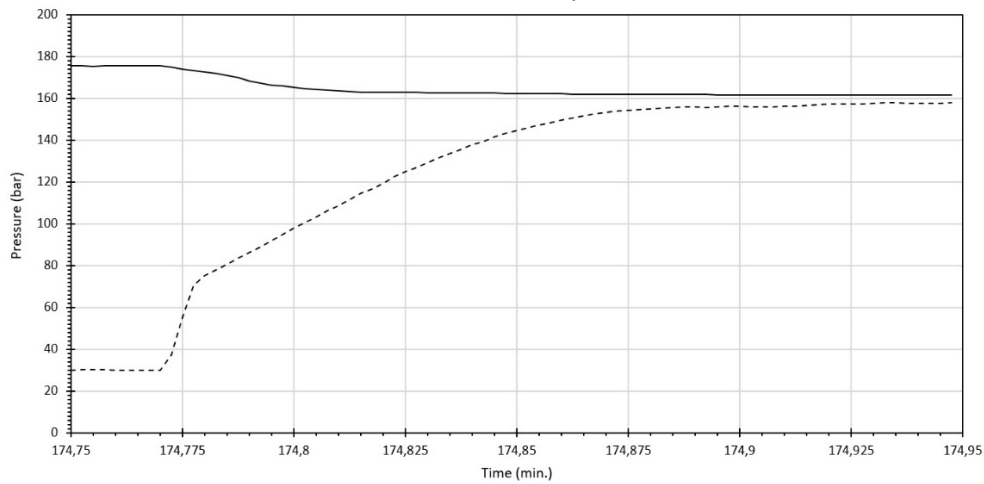
366 As it can be observed, the period of each charging cycle is around 24 min., and the
367 pressure at the inlet of the compressor changes from 15 bar to 29.5 bar, which is the set
368 point fixed at the control system to prevent failures. The compressor operates during
369 the descent ramp, while it remains off when this pressure increases. Close to 700 l of
370 hydrogen were stored at the stationary GSS during this test, increasing its pressure from
371 168 bar to 176 bar. The fast decrease in the pressure at the stationary GSS between
372 minutes 174 to 175 is due to the refueling of the GSS of the FCHEV. A zoom for this time
373 window is observed in Fig. 11 b) where this performance is clearly depicted. In the
374 different tests performed, the fast refueling time of the WEH system was demonstrated.
375 In this specific test, the GSS of the FCHEV is refilled from 30 bar to 157 bar in less than
376 20 s (dashed line), and the pressure at the stationary GSS of the hydrogen production
377 station change in less than 14 bar, from 175.5 bar to 161.6 bar (solid line). From the tests
378 performed, it was shown that the refilling frequency of the GSS of the FCHEV is every
379 1.5 days, while 11.5 hours are needed to refuel the used hydrogen in the stationary GSS.



380

381

a)



382

383

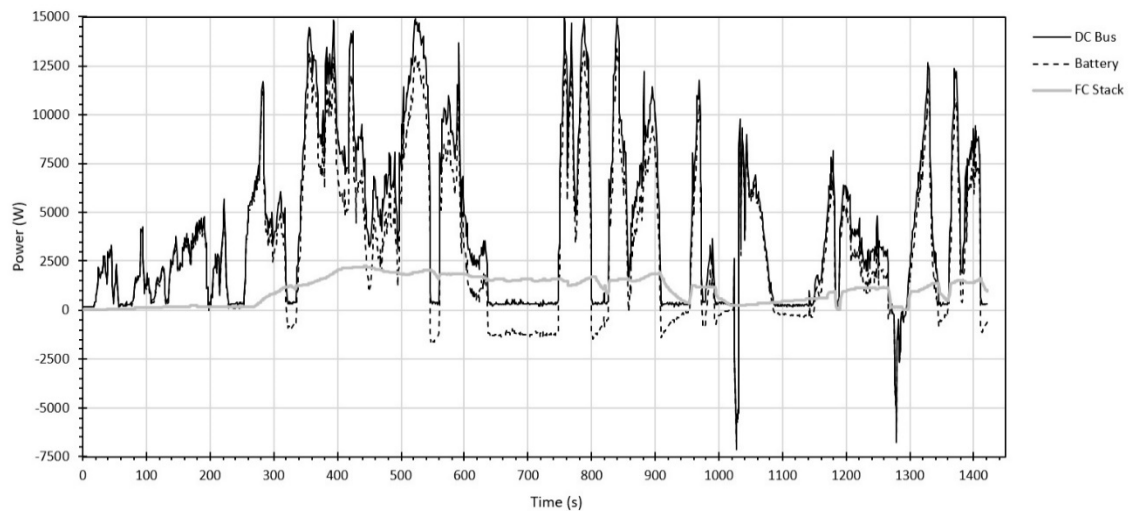
b)

384 Figure 11. Performance of both the system to refill hydrogen to the stationary GSS (a),
 385 and that to refuel hydrogen to the GSS of the FCHEV (b)

386 3.3. Performance of the hybrid electric car

387 Different field tests of the FCHEV were performed in real operating conditions at
 388 the winery. The results obtained during a real driving test are depicted in Fig. 12. It
 389 consisted in a round trip of 6 km that lasted around 24 min, from the parking of the
 390 winery to the vineyards, climbing two small hills. The average velocity of the FCHEV
 391 during the whole test was 15.2 km h^{-1} , reaching a maximum of 45 km h^{-1} with an average
 392 power demanded by the EM of the vehicle of 4.19 kW. However, as can be observed in
 393 Fig 12 a), the peak power demanded by the EM (solid black line) when ascending the
 394 hills or during a fast acceleration exceeds, by far, the rated power of the electric motor
 395 (7.5 kW). For the high demand range, the power is mainly supplied by the battery
 396 (dashed line), while for the low power demand range the CHARGING mode at the H-

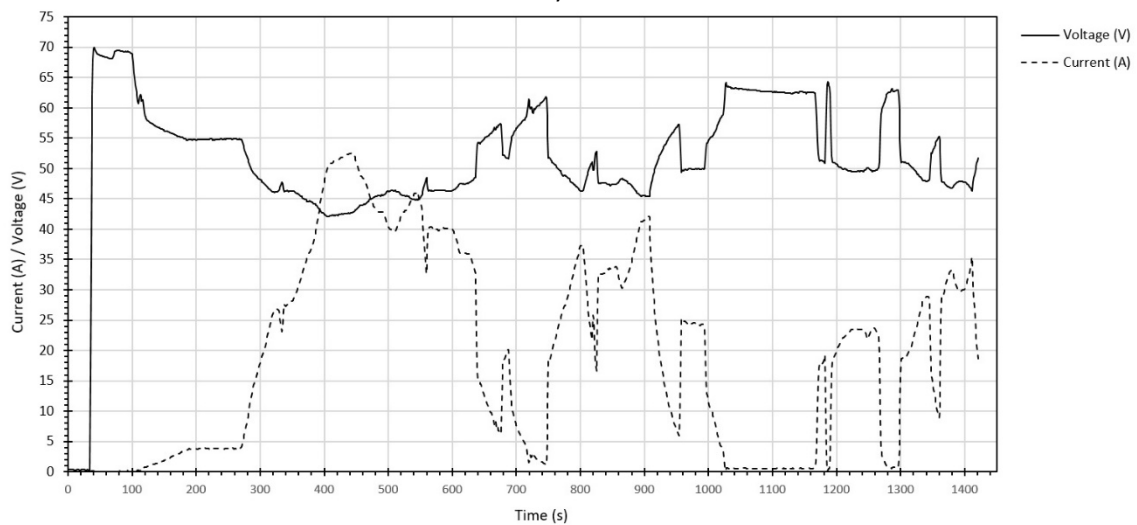
397 3000 stack is activated and part of the energy is used to recharge the battery. This
 398 situation corresponds to the different zones in Fig. 12 a) where the power of the battery
 399 is negative. When working in hybrid mode, 74.8% of the total energy demanded by the
 400 vehicle was supplied by the battery and 25.2% by the PEMFC.



401

402

a)



403

404

b)

405 Figure 12. Results of the real driving test in the winery: a) power of the different
 406 sources, and b) electric performance of the stack

407 On the other hand, the PEMFC stack works in a quasi-steady state (solid bold grey
 408 line), with an average power of 1.05 kW and a net efficiency of 51.4%. This result shows
 409 the excellent performance of the stack control system, avoiding sudden changes in load
 410 that can damage the device due to its slow dynamics. The average voltage of the H-3000
 411 PEMFC stack in this test is 51.8 V, and the average current reaches 20.3 A, which

412 corresponds to a current density of around 0.1 A cm^{-2} (see Fig 12 b). An interesting result
413 was to confirm that part of the kinetic energy of the FCHEV is recovered when braking,
414 corresponding with the two narrow negative peaks of power in times 1,028 s and 1,280
415 s. This unexpected performance, not indicated by the manufacturer in the vehicle
416 manual, occurs when the car is moving at a fast velocity (descending the second hill) and
417 the traction system is shifted to the lowest gear. Under this condition, the DC/AC
418 booster electronic converter of the EM can also work as a generator. Finally, it was also
419 confirmed that the actual range of the vehicle was almost doubled, from 2.7 hours for
420 the pure BEV to 4.8 hours of the hybrid one.

421 **3.4. Cost analysis of the electricity production**

422 Based on the publications of the Solar Energy Industry Association, the average
423 price of a complete PV system has dropped by more than 70% since the beginning of
424 2011 [35]. It is important to highlight that the PV plant of this project is not a typical
425 commercial facility, but it is a “demonstrative prototype”. Obviously, the replication of
426 the proposed solutions is cheaper than the prototype. In most cases a fixed array, which
427 is the conventional technology, should only be considered. The inclusion of the tracking
428 array and the floating panels increases the final cost, but it allowed showing and testing
429 the performance of the three systems under the same operating conditions. The same
430 demonstration purposes justified the incorporation of the hydrogen production facility
431 and the fuel-cell-powered vehicle despite their high cost, but the production and use of
432 hydrogen is not considered for this economic comparison.

433 In the cost analysis, the three technologies that are commonly used to supply
434 electric power to the WWTP and to the pumping system for irrigation in the wine
435 industry are compared. These are, namely, the commercial electric grid, a diesel-based
436 generation set (genset), and the PV solar plant. It is noteworthy that the aim of the
437 calculations is to compare the three solutions, because the supply of energy is needed
438 in any case. The cost of all the equipment and the increase in fuel prices have been
439 considered, using the data from the last 15 years. In the case of the PV facility, the costs
440 inherent to the building work for the three arrays, the air conditioning system of the
441 technical room, and the assembling of the whole plant are also included. Besides, a
442 degradation rate of 1% is considered for the solar panels. To calculate the annual costs

443 of the three technologies, the following equations are used,

$$444 \quad TAC_{PV} = I_{O-PV} + \left[\sum_{Year=1}^n AE_{Year} (1 + Inf_{gen})^{Year} \right] + CoL_{Bat} + CoL_{Inv}, \quad (1)$$

$$445 \quad TAC_{DG} = I_{O-DG} + \left[\sum_{Year=1}^n AE_{Year} (1 + Inf_{gen})^{Year} + Co_{DG} (1 + Inf_{DG})^{Year} + CoL_{DG} \right], \quad (2)$$

$$446 \quad TAC_{CE} = I_{O-DG} + [(CoE \cdot E_{cons}) + (CoP \cdot P_{cons}) + Taxes](1 + Inf_{CE})^{Year}, \quad (3)$$

447 where TAC is the total annual costs (€), I_o the initial investment costs (€), AE the annual
 448 expenses (€), Inf the inflation (%), CoL the cost due to lifetime (€), CoE the energy cost
 449 (€), CoP the power cost (€), E the energy consumed (kWh), and P the power consumed
 450 (kW). Subscript PV refers to the solar PV plant, DG to the diesel genset, CE to the
 451 electricity from the commercial grid, gen to general, Bat to the battery bank, and Inv to
 452 the inverters. Besides, the net present value (NPV) is calculated according to

$$453 \quad NPV = \sum_{Year=1}^n \frac{C_{Year}}{(1+k)^{Year}} - I_o, \quad (4)$$

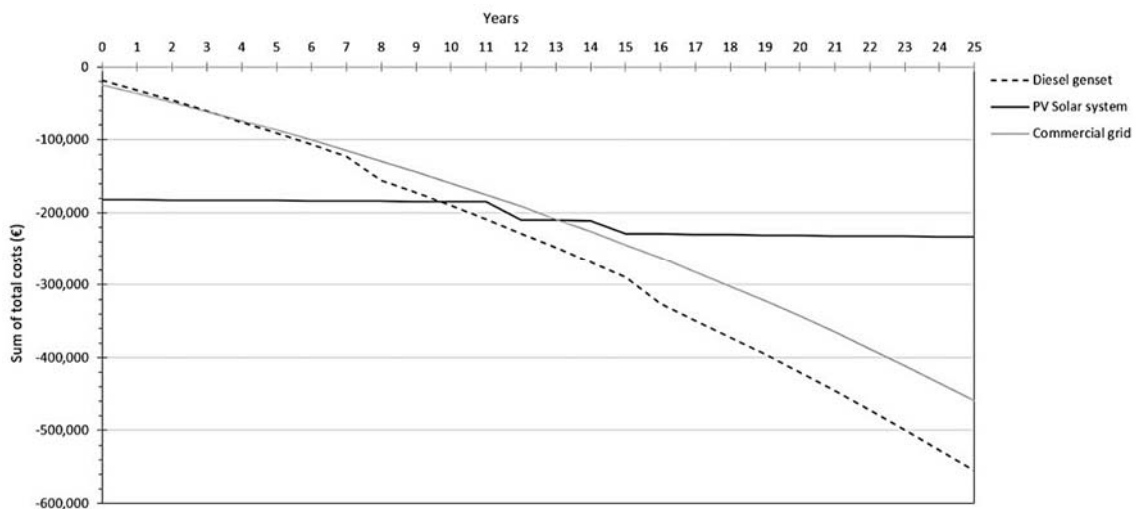
454 in which C is the yearly cash-flow, and k is the annual discount rate considered (10%). A
 455 summary of the main parameter used in the analysis is listed in Table 4.

Parameters	Diesel genset	Electricity grid	PV solar plant
Annual energy consumption (kWh)		75,000.00	
Total electric power (kW)		50	
Fuel oil price (€ l ⁻¹)		0.60	
Initial investments (all costs included)	18,500.00	25,000.00	181,854.00
Annual costs:			
- Maintenance (€)	1,846.63		250.00
- Fuel oil (€)	11,079.00		
- Electric energy index (€ kWh ⁻¹)		0.11245	
- Electric power index (€ kW ⁻¹)		45.7245	
- Renting devices (€)		343.35	
- Taxes in Spain (€)		526.70	
Inflation			
- General (%)	3.00	3.00	3.00
- Diesel (%)	3.20		
- Electricity (%)		3.20	

456 Table 4. Main parameters used in the cost analysis

457 The evolution of the annual costs of the three systems for the values considered in
 458 the study is presented in Fig. 13. The total cost of the PV solar system is almost constant
 459 because it is mainly affected by the initial investment cost (181,854.00 €). Nevertheless,
 460 the maintenance cost, as well as the costs related to the lifetime of both the battery
 461 bank (12 years) and the inverters (15 years) have also been included in the analysis. A
 462 lifetime of 15 years, and its corresponding cost, was also considered for the diesel

463 genset. As can be observed, from years 9.5 and 13 the costs of both the diesel-based
 464 generation system and the commercial electricity, respectively, are greater than the PV
 465 solar power system. A positive result of the NPV (58,086.31 €) was only obtained for the
 466 PV solar power system, with an internal rate of return (IRR) of 13.44%. The NPV values
 467 obtained for the diesel system and for conventional electricity are -187,819.93 € and
 468 -161,121.15 €, respectively. So, the profitability of the PV solar power system is clearly
 469 demonstrated.



470
 471 Figure 13. Cost analysis for the three technologies commonly used to produce
 472 electricity in the wine industry

473 4. Conclusions

474 The technical and economic feasibility of an isolated electrical plant from PV solar
 475 energy that eliminates both local diesel-based generation equipment and aerial power
 476 lines has been demonstrated in Viñas del Vero winery. With the facility developed in the
 477 present research, during the first year around 72 MWh of electricity were produced,
 478 saving the emission of around 24 tons of CO₂-e to the atmosphere. Besides, 6.4 MWh
 479 have been employed to produce hydrogen in a generation and refueling station
 480 specifically designed and manufactured for this project. During the first year, 1,214 Nm³
 481 of hydrogen have been produced, avoiding the emission of close to 3 tons of CO₂-e. Field
 482 tests performed to the FCHEV proved that when working in hybrid mode around 30% of
 483 the total energy demanded was supplied by the PEMFC stack, which notably extend the
 484 original range. The excellent performance of the commercial WEH refueling system was
 485 also demonstrated.

486 Considering the efficiency of the different elements of the system, the overall
487 efficiency for the electricity conversion of the power-to-gas-to-power plant (from the PV
488 panels to the vehicle wheels) ranges from 24.6% (when the electricity to produce
489 hydrogen is directly obtained from the PV panels) to 30.5% (when the electricity is
490 previously stored in the battery bank). Even when the present PV power plant is a
491 demonstrative prototype, a positive result has been obtained for both the NPV and the
492 IRR, demonstrating the profitability of the investment. This is a very important result to
493 encourage the investment of private capital in the renewable energy sector.

494 **Acknowledgements**

495 This work has been funded by the European Union LIFE+ under project LIFE13
496 ENV/ES/000280, and by the Secretariat of State for Research of the Spanish Ministry of
497 Economy and Competitiveness under project DPI2015-69286-C3-1-R (MINECO/FEDER,
498 UE). Support of the Regional Government of Aragon to the Experimental Fluid Dynamics
499 Research Group (T03) of the LIFTEC is also acknowledged.

References

- [1] G. Gahleitner, Hydrogen from renewable electricity: An international review of power-to-gas pilot plants for stationary applications, *International Journal of Hydrogen Energy* (2013) 38, 2039-2061
- [2] Y.S. Mohammed, M.W. Mustafa, N. Bashir, Hybrid renewable energy systems for off-grid electric power. Review of substantial issues, *Renewable and Sustainable Energy Reviews* (2014) 35, 527-539
- [3] S.E. Hosseini, M.A. Wahid, Hydrogen production from renewable and sustainable energy resources: promising green energy carrier for clean development, *Renewable and Sustainable Energy Reviews* (2016) 57, 850-866
- [4] D. Scamman, M. Newborough, H. Bustamante, Hybrid hydrogen-battery systems for renewable off-grid telecom power, *International Journal of Hydrogen Energy* (2015) 40, 13876-13887
- [5] F. Yilmaz, M. Tolga Balta, R. Selbaş, A review of solar based hydrogen production methods, *Renewable and Sustainable Energy Reviews* (2016) 56, 171–178
- [6] X. Wu, X. Hu, S. Moura, X. Yin, V. Pickert, Stochastic control of smart home energy management with plug-in electric vehicle battery energy storage and photovoltaic

- array, *Journal of Power Sources* (2016) 333, 203-212
- [7] D.B. Nelson, M.H. Nehrir, C. Wang, Unit sizing and cost analysis of stand-alone hybrid wind/PV/fuel cell power generation systems, *Renewable Energy* (2006) 31, 1641-1656
- [8] C. Wang, M.H. Nehrir, Power management of a stand-alone wind-photovoltaic-fuel cell energy system, *IEEE Transactions on Energy Conversion* (2008) 23, 957-967
- [9] M. Uzunoglu, O.C.Onar, M.S. Alam, Modeling, control and simulation of a PV/FC/UC based hybrid power generation system for stand-alone applications, *Renewable Energy* (2009) 34, 509-520
- [10] S. Mumtaz, L. Khan, Adaptive control paradigm for photovoltaic and solid oxide fuel cell in a grid-integrated hybrid renewable energy system, *PLoS ONE* (2017) 12(3), e0173966
- [11] A. Andrijanovits, H. Hoimoja, D. Vinnikov, Comparative Review of Long-Term Energy Storage Technologies for Renewable Energy Systems, *Electronics and Electrical Engineering* (2012) 2(118), 21-26
- [12] A. Yilanci, I. Dincer, H.K. Ozturk, A review on solar-hydrogen/fuel cell hybrid energy systems for stationary applications, *Progress in Energy and Combustion Science* (2009) 35, 231-244
- [13] R. Mustata, V. Roda, A. Nuevo, L. Valiño, A. Lozano, F. Barreras, J.L. Bernal, J. Carroquino, Small scale demonstration project for the production and use of hydrogen from renewable energy sources in the wine sector, *Proceedings of the 21st World Hydrogen Energy Conference, WHEC* (2016) 383-384
- [14] J. Carroquino, R. Dufo-López, J.L. Bernal-Agustín, Sizing of off-grid renewable energy systems for drip irrigation in Mediterranean crops, *Renewable Energy* 76 (2015) 566-574
- [15] J. Aymamí, A. García, O. Lacave, L. Lledó, M. Mayo, S. Parés, Analysis of the resource. Wind Atlas of Spain. Technical Study PER 2011-2020, Spanish Institute for the Diversification and Saving of Energy (IDEA), Madrid, 2011 (in Spanish)
- [16] Atlas of solar radiation in Spain, Meteorological Agency (AEMET), 2012, in: http://www.aemet.es/es/serviciosclimaticos/datosclimatologicos/atlas_radiacion_solar (in Spanish)

- [17] PVGIS - Online free solar photovoltaic electricity generator simulation and solar radiations maps. Consulted in July 2017 at the webpage: <http://photovoltaic-software.com/pvgis.php>
- [18] E. Dursun, B. Acarkan, O. Kilic, Modeling of hydrogen production with a stand-alone renewable hybrid power system International Journal of Hydrogen Energy 37 (2012) 3098-3107
- [19] D. Ghribi, A. Khelifa, S. Diaf, M. Belhamel, Study of hydrogen production system by using PV solar energy and PEM electrolyser in Algeria, International Journal of Hydrogen Energy 38 (2013) 8480-8490
- [20] R. Lacko, B. Drobnič, M. Sekavčnik, M. Mori, Hydrogen energy system with renewables for isolated households: The optimal system design, numerical analysis and experimental evaluation, Energy and Buildings 80 (2014) 106-113
- [21] T.C. Morales, V.R. Oliva, L.F. Velázquez, Hydrogen from renewable energy in Cuba, Energy Procedia 57 (2014) 867-876
- [22] D. Laslett, C. Carter, C. Creagh, P. Jennings, "A large-scale renewable electricity supply system by 2030: Solar, wind, energy efficiency, storage and inertia for the South West Interconnected System (SWIS) in Western Australia", Renewable Energy, 113 (2017) 713-731
- [23] A. Aly, S. S. Jensen, A.B. Pedersen, Solar power potential of Tanzania: Identifying CSP and PV hot spots through a GIS multicriteria decision making analysis, Renewable Energy 113 (2017) 159-175
- [24] M.R. Maghami, S.N. Asl, M.E. Rezadad, N.A. Ebrahim, C. Gomes, Qualitative and quantitative analysis of solar hydrogen generation literature from 2001 to 2014, Scientometrics 105 (2015) 759-771
- [25] S. Sonwani, R. Prasad, Low-cost renewable hydrogen production using solar photovoltaic panel, Current Science 111 (2016) 712-716
- [26] Z. Su, S. Ding, Z. Gan, X. Yang, Analysis of a photovoltaic-electrolyser direct-coupling system with a V-trough concentrator, Energy Conversion and Management 108 (2016) 400-410
- [27] F. Barbir, Hydrogen Islands-Utilization of Renewable Energy for an Autonomous Power Supply, Hydrogen Science and Engineering: Materials, Processes, Systems and Technology 2 (2016) 1075-1096

- [28] F. Sayedin, A. Maroufmashat, S. Sattari, A. Elkamel, M. Fowler, Optimization of photovoltaic electrolyzer hybrid systems; taking into account the effect of climate conditions, *Energy Conversion and Management* 118 (2016) 438-449
- [29] V. Dash, P. Bajpai, Power management control strategy for a stand-alone solar photovoltaic-fuel cell-battery hybrid system, *Sustainable Energy Technology Assessments* 9 (2015) 68-80
- [30] iHOGA website. Available at: <http://personal.unizar.es/rdufo/index.php?lang=en>
- [31] Sh. Sreekumar, A. Benny, Maximum power point tracking of photovoltaic system using fuzzy logic controller based boost converter, *Proceedings of the IEEE International Conference on Current Trends in Engineering and Technology, ICCTET'13, Coimbatore, India (2013)* 275–280
- [32] V. Roda, J. Carroquino, L. Valiño, A. Lozano, F. Barreras, Remodeling of a commercial plug-in battery electric vehicle to a hybrid configuration with a PEM fuel cell, *International Journal of Hydrogen Energy* <https://doi.org/10.1016/j.ijhydene.2017.12.171>
- [33] Bulletin of the energy situation in Aragon and the regional energy balances in the period 1998-2004. Department of Economics, Industry and Employment, Aragon's Institute of Statistics (IAEST), November 18th, 2016, in Spanish
- [34] Emission Factors. Carbon Footprint Registry, Compensation and absorption Projects for Carbon Dioxide, report of the Spanish Ministry of Agriculture and Fisheries, Food and Environment, version 9, July 2017, in Spanish
- [35] Web site: <http://www.seia.org/research-resources/solar-industry-data>, consulted in August 2017